

EFFECT OF LIQUID FUEL DROPLET SIZE ON SOOT EMISSION FROM TURBULENT SPRAY FLAMES*

I. ZAHMATKESH** AND M. MOGHIMAN

Faculty of Mechanical Engineering, Ferdowsi University of Mashhad, Mashhad, I. R. of Iran
Email: Zahmatkh@shirazu.ac.ir

Abstract– The present study is concerned with the effect of fuel droplet size on the complex soot process in a turbulent liquid-fuelled combustor. A hybrid Eulerian-Lagrangian method is employed to model the reactive flowfield inside the combustor. Equations governing the gas phase are solved by a control-volume based semi-implicit iterative procedure, while the time-dependent differential equations for each size of the fuel droplets are integrated by a semi-analytic method. The processes leading to soot consist of both formation and combustion. Soot formation is simulated using a two-step model, while a finite rate combustion model with the eddy dissipation concept is implemented for soot combustion. Also, mathematical models for turbulence, combustion, and radiation are used to take into account the effects of these processes. Results reveal the significant influence of liquid fuel droplet size on soot emission from turbulent spray flames under different equivalence ratios, inlet air temperatures, and combustor wall temperatures. The predictions show that reduction of spray droplet size considerably decreases soot emission from spray flames.

Keywords – Spray combustion, soot formation, droplet size

1. INTRODUCTION

Combustion of hydrocarbon fuels generally produces soot particles which have important technological, environmental, health, and economic implications. It is well known that flame generated soot particles considerably enhance radiation heat transfer [1] which affects thermal efficiencies. Deposition of soot particles on the combustor wall reduces its durability. Furthermore, soot emission to the atmosphere from various combustion sources contributes to air pollution levels and global warming. Also, long-term exposure to these nanometer-size aerosols has recently been linked to severe adverse effects on human health since these extremely small size particles can be inhaled deeply into the lungs. Finally, soot has a poorly understood complex relationship with other undesirable pollutants such as polycyclic aromatic hydrocarbons (PAHs) and NO_x [2]. These technological and environmental concerns emphasize the need for a deep understanding of the soot process.

The process of soot evolution from hydrocarbon fuels consists of complex chemical and physical steps, including fuel pyrolysis, formation of polycyclic aromatic hydrocarbons, particle inception, coagulation, surface growth, carbonization, agglomeration, and oxidation [3]. Many authors have investigated the effect of different parameters on soot emission experimentally and numerically [4-6].

Typically, flames of liquid fuels have greater soot emission than the gaseous fuels which is a direct result of the diffusion character of these types of flames. Therefore soot process in these types of flames must be considered more precisely. The soot process in spray flames is closely related to atomization, penetration, heating up, and evaporation of droplets. This makes the study of soot formation in spray

*Received by the editors September 5, 2005; final revised form February 26, 2006.

**Corresponding author

combustion a challenging task. Although many authors have investigated spray structure and combustion inside spray flames [7-9], the effect of droplet size on soot formation and emission is not well studied and documented up to now. The only available work goes back to the experimental investigation of Lefebvre [10] which has reported the establishment of a very rich primary zone for the lower size droplets that increase soot formation there. The aim of the present work is the prediction of soot emission from turbulent spray flames and the investigation of the effect of spray droplet size on fuel penetration, evaporation, combustion, and soot formation. The computations are conducted under different operating conditions including various equivalence ratios, inlet air temperatures, and combustor wall temperatures.

2. THEORETICAL FORMULATION

a) Physical system and assumptions

The physical system refers to the evaporation and combustion of a continuously injected liquid fuel spray in a combustor. The air enters the combustor with a swirl while the liquid fuel is sprayed on it. The following assumptions have been made in the present study:

- The fuel spray is considered to consist of a finite size range, with the size distribution specified by the Rosin–Rammler function.
- A one-way interaction model is used for the gas flow and the droplets trajectory analysis. That is, it is assumed that air carries the droplets, but they have no effect on the air flow.
- Buoyancy forces are neglected.
- Effects of virtual mass force and Basset force on the droplets are not considered due to high-density ratio between the phases.
- There is no nucleation, collision, break-up, coagulation, or micro-explosion of the droplets.
- The droplets do not take part in radiative energy exchange.
- The liquid fuel is considered to be cetane.

b) Numerical model

The numerical model is based on a typical Eulerian gas phase and a Lagrangian droplet phase formulation. Since a one-way interaction model is used for the gas flow and the droplets trajectory analysis, the air flowfield is first evaluated while the results are used for the evaluation of the droplets trajectories.

1. Gas phase conservation equations: The average gas phase equations are as follows:

Continuity:

$$\frac{\partial u}{\partial x} + \frac{1}{r} \frac{\partial}{\partial r}(rv) = \dot{S} \quad (1)$$

Momentum:

$$\frac{1}{r} \left[\frac{\partial}{\partial x}(r\rho uu) + \frac{\partial}{\partial r}(r\rho uv) \right] = -\frac{\partial p}{\partial x} + \mu \nabla^2 u - \frac{1}{r} \frac{\partial}{\partial r}(r\rho \overline{u'v'}) - \frac{\partial}{\partial x}(\rho \overline{u'u'}) \quad (2)$$

$$\frac{1}{r} \left[\frac{\partial}{\partial x}(r\rho uv) + \frac{\partial}{\partial r}(r\rho vv) - \rho w^2 \right] = -\frac{\partial p}{\partial r} + \mu \left(\nabla^2 v + \frac{v}{r^2} \right) - \frac{1}{r} \frac{\partial}{\partial r}(r\rho \overline{v'v'}) - \frac{\partial}{\partial x}(\rho \overline{u'v'}) - \frac{1}{r} \rho \overline{w'w'} \quad (3)$$

$$\frac{1}{r} \left[\frac{\partial}{\partial x}(r\rho vw) + \frac{\partial}{\partial r}(r\rho vw) + \rho vw \right] = \mu \left(\nabla^2 w - \frac{w}{r^2} \right) - \frac{1}{r} \frac{\partial}{\partial r}(r\rho \overline{v'w'}) - \frac{\partial}{\partial x}(\rho \overline{u'w'}) - \frac{1}{r} \rho \overline{v'w'} \quad (4)$$

In view of the inability of the $k-\varepsilon$ model to cope with anisotropic flows [11], the turbulent stresses are calculated from an algebraic stress model [12]. Also, a conventional wall-function approach is used in the near-wall region to bridge the viscous sublayer in such a way that the first grid points from the walls be located in a region with an appropriate y^+ .

Energy:

$$\frac{1}{r} \left[\frac{\partial}{\partial x} (r\rho u h) + \frac{\partial}{\partial x} (r\rho v h) \right] = \Gamma_h \nabla^2 h - \frac{1}{r} \frac{\partial}{\partial r} (r\rho \overline{v'h'}) - \frac{\partial}{\partial x} (\rho \overline{u'h'}) + \dot{S}_h \quad (5)$$

The energy source term (\dot{S}_h) has two components. One of which is the net energy absorbed by the exchange of radiation which is evaluated from Gosman and Lockwood [13]

$$\dot{S}_h = 2a \times [R_x + R_r - 2E_b] \quad (6)$$

Where, R_x and R_r are the radiant fluxes determined by the solution of two differential equations

$$\frac{d}{dx} \left[\Gamma_x \frac{dR_x}{dx} \right] + a(E_b - R_x) + \frac{s}{4}(R_r - R_x) = 0 \quad (7)$$

$$\frac{1}{r} \frac{d}{dx} \left[r \left(\Gamma_r \frac{dR_r}{dx} \right) \right] + a(E_b - R_x) + \frac{s}{4}(R_r - R_x) = 0 \quad (8)$$

The second component in the energy source term is the energy generated due to chemical reaction. The energy addition due to combustion is determined in consideration of a single step, irreversible, global reaction between the fuel vapor and oxygen following a finite rate chemistry as:



In this study, the reaction rates that appear as source terms in species transport equations (Eq. (12)) are computed by using the eddy dissipation concept [14].

$$\dot{S}_j = A\rho \frac{\varepsilon}{k} \min[m_F s_F, m_{O_x}] \quad (10)$$

The gas phase equations are completed by the ideal equation of state which determines the distribution of density as:

$$\rho = \frac{P}{RT} \left[\sum \frac{m_j}{M_j} \right] \quad (11)$$

This assumption is appropriate since the high temperatures associated with combustion generally result in sufficiently low densities for ideal gas behavior to be a reasonable approximation.

Individual species conservation:

$$\frac{1}{r} \left[\frac{\partial}{\partial x} (r\rho u m_j) + \frac{\partial}{\partial r} (r\rho v m_j) \right] = \Gamma_{mj} \nabla^2 m_j - \frac{1}{r} \frac{\partial}{\partial r} (r\rho \overline{v'm_j'}) - \frac{\partial}{\partial x} (\rho \overline{u'm_j'}) + \dot{S}_j \quad (12)$$

In this study, the species conservation equation is solved for fuel vapor, oxygen, carbon-dioxide and soot. The conservation equation for each species contains a source term related to the chemical reaction which is negative for fuel vapor and oxygen, but positive for carbon-dioxide. The equation for fuel vapor contains an additional source term to take care of the fuel mass evaporated from the droplets. The influence of soot formation and combustion on, respectively, fuel and oxygen mass fractions is accounted

for by a sink term added to the conservation equation of each of these species. A source term due to soot combustion is added to the CO₂ conservation equation.

Soot Formation

The soot process consists of both formation and combustion. Since the capability of the soot model proposed by Tesner *et al.* [15] has been widely accepted [16-17], in this study the formation of soot is calculated by this model. The model solves two transport equations, one equation for particle nucleation/combustion, and the second for soot formation/combustion.

The source term for the nuclei transport equation is the net rate of nuclei generation and is given by

$$\dot{S}_N = \dot{S}_{N,F} - \dot{S}_{N,C} \quad (13)$$

Where, the rate of nuclei formation depends on the spontaneous formation and branching processes, described by

$$\dot{S}_{N,F} = \eta_0 + \rho[(F - G)m_N - \lambda_0 \rho m_N m_S] \quad (14)$$

Here

$$\eta_0 = A_0 \rho^n m_F^n \exp(-E/RT) \quad (15)$$

The rate of nuclei combustion is assumed to be proportional to the rate of soot combustion

$$\dot{S}_{N,C} = \dot{S}_{S,C} \frac{m_N}{m_S} \quad (16)$$

Where the soot combustion rate ($\dot{S}_{S,C}$) is given by Eq. (19).

Also, the source term for the soot transport equation (\dot{S}_S) is calculated according to

$$\dot{S}_S = \dot{S}_{S,F} - \dot{S}_{S,C} \quad (17)$$

Where

$$\dot{S}_{S,F} = \rho M_p (\alpha - \beta \rho m_S) m_N \quad (18)$$

The rate of soot combustion (oxidation) is calculated by the Magnussen and Hjertager model [14]

$$\dot{S}_{S,C} = A \rho \frac{\varepsilon}{k} \min \left[m_S, \frac{m_O}{s_S} \frac{m_S s_S}{m_S s_S + m_F s_F} \right] \quad (19)$$

The effect of soot, which is usually the dominant radiating species in hydrocarbon-fueled flames [1], on the radiative heat transfer inside the combustor is accounted for by using a modified absorption coefficient (a) of the gas as:

$$a_m = a + b_1 \rho m_S [1 + b_T (T - 2000)] \quad (20)$$

2. Generation of droplet phase information: The velocity, mass and temperature history of all droplet groups along their trajectories are obtained from the respective conservation equations on a Lagrangian frame similar to Sharma and Dom [18]

Droplet velocity:

The drag coefficient (C_D) is computed following the standard drag law as given by Hinds [19]. Also, the effect of gas phase turbulence on the droplets motion is simulated using a stochastic approach [18].

$$\frac{du_i^d}{dt} = \frac{3\mu C_D \text{Re}}{4\rho_p D_p^2} (u_i^g - u_i^d) \quad (21)$$

Droplet mass:

$$\frac{dm^d}{dt} = -\pi\rho^2 d^2 \beta (m_{F,s} - m_F) \quad (22)$$

Droplet temperature:

$$m^d c_p^d \frac{dT^d}{dt} = \pi d^2 h (T - T^d) + \frac{dm^d}{dt} \Delta H_v \quad (23)$$

Where, ΔH_v is the enthalpy of vaporization of the liquid fuel. Mass transfer coefficient (β) and heat transfer coefficient (h) in Eqs. (22) and (23) respectively, are evaluated from

$$Sh = \frac{2 + 0.6 \text{Re}_d^{0.5} Sc^{0.33}}{1 + B} \quad (24)$$

$$Nu = \frac{2 + 0.6 \text{Re}_d^{0.5} Pr^{0.33}}{1 + B} \quad (25)$$

Eqs. (21), (22) and (23) are solved for V_i^d , m^d , and T^d respectively, with appropriate initial conditions.

The initial droplet size distribution of liquid fuel spray is assumed to follow the Rosin-Rammler distribution function given by

$$G'(d_i) = \frac{\exp(-bd_i^n) - \exp(-bd_{\max,i}^n)}{\exp(-bd_{\min,i}^n) - \exp(-bd_{\max,i}^n)} \quad (26)$$

where $G'(d_i)$ is the mass fraction of the spray droplets having a diameter above d_i . The dispersion parameter (n) is taken as used by Saario *et al.* [20].

Due to Faeth [21], ten droplet group sizes, ranging from 15 to 50 μm (for a spray with fine droplets) and 50 to 120 μm (for a spray with large droplets) are assumed for the calculation in the present model.

3. METHOD OF SOLUTION

a) Numerical scheme

The gas conservation equations are solved using a control-volume based computational procedure [22]. The convective terms are discretized by the power law scheme. Pressure linked equations are solved by the SIMPLE algorithm and the set of algebraic equations is solved sequentially with the line-by-line tridiagonal-matrix algorithm. The convergence criterion is determined by the requirement that the maximum value of the normalized of any equation must be less than 1×10^{-5} . Under-relaxation factor is chosen as 0.3 for all dependent variables except nuclei and soot, for which 0.4 is suitable. As in the previous work [23], this solution procedure has been modified for spray penetration and combustion, this paper concentrates on developing it for soot formation and combustion.

b) Numerical mesh

A numerical mesh of 120×68 grid nodes is used after several experiments, which shows that further refinement in either direction does not change the result (maximum difference in velocity and other scalar functions in the carrier phase) by more than 2%. The grid spacing in axial and radial directions are changed smoothly to minimize the deterioration of the formal accuracy of the finite difference scheme due

to variable grid spacing and in such a way that a higher concentration of nodes occur near the inlet and the walls.

c) Operating parameters and boundary conditions

Because of the elliptic nature of the conservation equations, boundary conditions are specified at all boundaries of the domain considered. The air enters the combustor with an axial velocity equal to 18 m/s. The swirl number of the inlet air is considered as:

$$Sw = \frac{\int_{r_1}^{r_2} 2\pi\rho u w r^2 dr}{r_2 \int_{r_1}^{r_2} 2\pi\rho u^2 r dr} = 1.24 \quad (27)$$

In this study, different inlet air temperatures are investigated. The k and ε profiles are specified using uniform distributions corresponding to a free stream turbulence intensity of $T_u = 5\%$. The liquid fuel is injected at 300 K and axially with a pressure-swirl atomizer in such a way that its axial velocity is 20 m/s and its tangential velocity is 14 m/s. Different equivalence ratios are investigated by testing different fuel flow rates. A zero axial gradient is prescribed at the outlet for all variables. Also, different temperatures are specified on the combustor walls.

4. RESULTS AND DISCUSSION

Numerical calculations are performed for a spray combustor with an internal diameter of 0.153 m and a length of 0.338 m. The computational procedure is first used to simulate the condition at which inlet air temperature equals 800 K. The fuel flowrate is determined in such a way that equivalence ratio is kept at 0.5. Temperature of the walls is assumed to be 1200 K. Also, the size range of the fuel droplets in spray is chosen to be in the range of 50 to 120 μm .

Figures 1 and 2 show the distribution of the gas phase velocity field and the temperature contours within the spray combustor for the specified condition from the solution of the present numerical model. It is observed from Fig. 1 that an internal recirculation zone (IRZ) is established near the central axis upstream from the combustor. This is due to the incoming swirling flow. Sudden expansion at the inlet also establishes a corner recirculation zone near the walls. The presence of the internal recirculating flow helps to stabilize the flame near the axis close to the inlet, as evident from the high temperature contours shown in Fig. 2. The flame spreads in the radial direction in the primary zone depending mainly upon the spray cone angle.

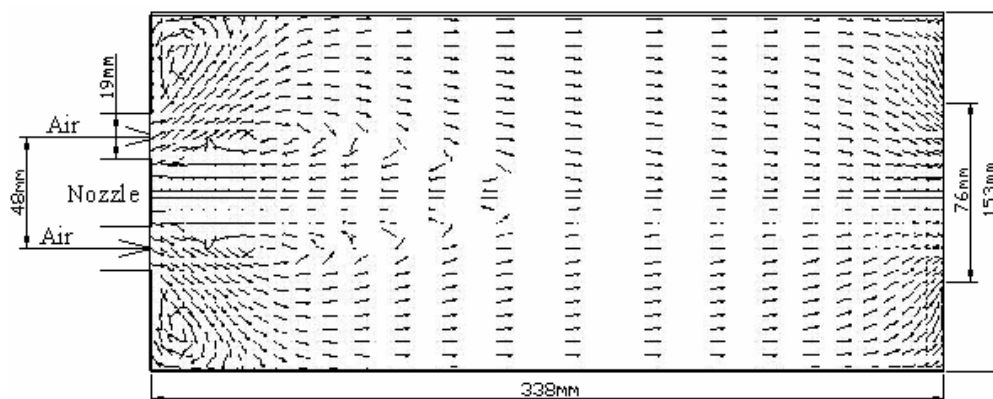


Fig. 1. The gas phase velocity field inside the combustor

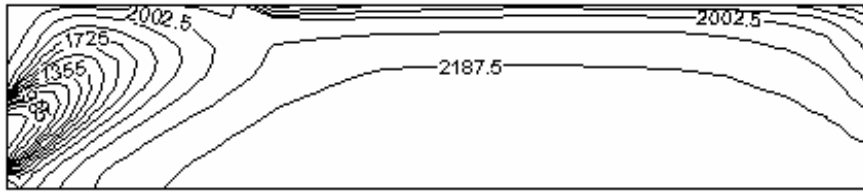


Fig. 2. Temperature (K) contours inside the upper half of the combustor

The accuracy of the quantitative or even the qualitative trends of the results depends on the accuracy with which velocity, temperature, and species concentration fields are determined from the numerical computation. To establish the accuracy of the present study, a possible comparison between velocity and temperature distributions predicted by the computational model is made with the experimental work of Khalil [24] under a similar condition. It is observed that the predicted axial and tangential velocity components agree fairly well with the experimental results (Fig. 3). The discrepancy between the two results can be due to turbulence modeling, which shows that further works can be applied. Similar trends can be observed from the comparison between the temperature distribution predicted by this model and the experimental results (Fig. 4). The discrepancy can be attributed to the fundamental assumption made in the combustion model used (Magnussen and Hjertager model [14]) which relates the rate of combustion with turbulent energy and dissipation.

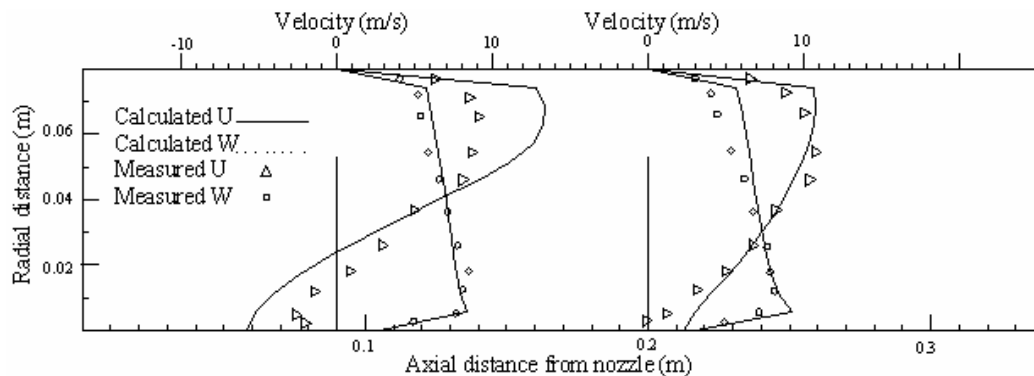


Fig. 3. Comparison of the predicted axial and tangential velocity distributions with experimental data

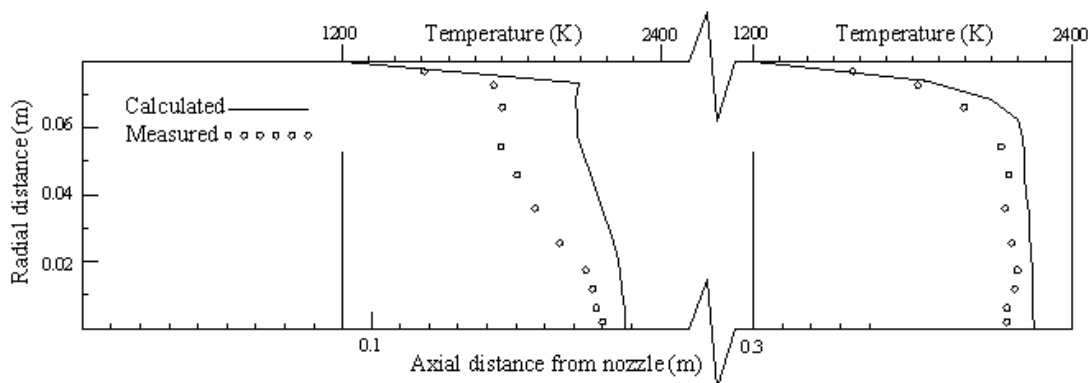


Fig. 4. Comparison of the predicted temperature distributions with experimental data

Figure 5 shows the trajectories of individual evaporating droplets in the upper half of the combustor. It is seen that the smallest sizes evaporate completely in the vicinity of the point of the issue, whereas it takes time for the larger droplets to heat up, reach the boiling point, and vaporize completely. Thus, the

larger fuel droplets penetrate longer axial distances in the combustor. Also, some of the droplets may be so large that they hit the cylindrical wall of the combustor before they vaporize completely [23].

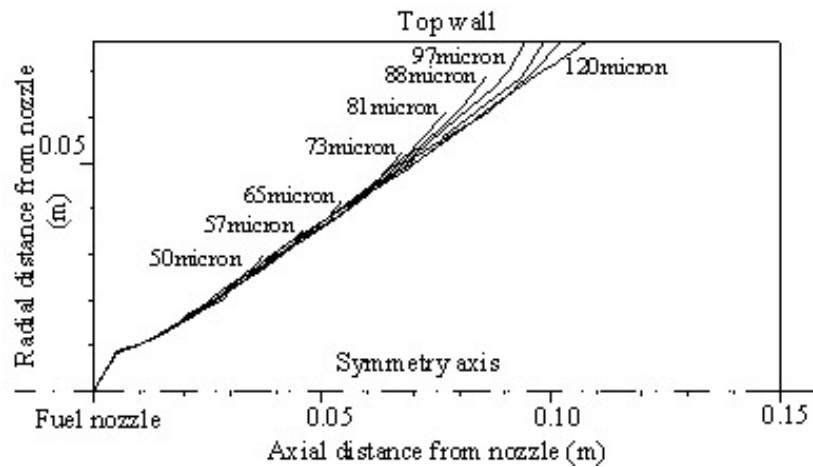


Fig. 5. Trajectories of the fuel droplets in the upper half of the combustor

To investigate the effect of fuel droplet size on the formation and emission of soot under different conditions, equivalence ratios, inlet air temperatures, and wall temperatures are changed and the results for the two aforementioned droplet group sizes are compared with each other.

Figures 6 and 7 represent the centerline distributions of fuel vapor and temperature for the two droplet group sizes. As it is clear from Fig. 6, using the fine droplets (ranging in size from 15 to 50 μm) concentrates fuel vapor upstream of the combustor. This is due to faster heating up and vaporization of the fine droplets (Fig. 5), which leads to an increase in temperature in the vicinity of the point of the issue which can be observed from Fig. 7. The trends in the distributions of temperature and fuel vapor mass fraction shown above affect the distribution of soot along the combustor as displayed in Fig. 8. The comparison of the soot mass fraction obtained for the two droplet group sizes reveals that the fine droplets produce higher soot in the inlet area of the combustor, while along the combustor soot formation is higher for the large droplets. Thus, soot emission (averaged soot mass fraction in the outgoing gases) in the spray with the large droplets is higher, which is in agreement with the results of previous studies of Leffbvre [10].

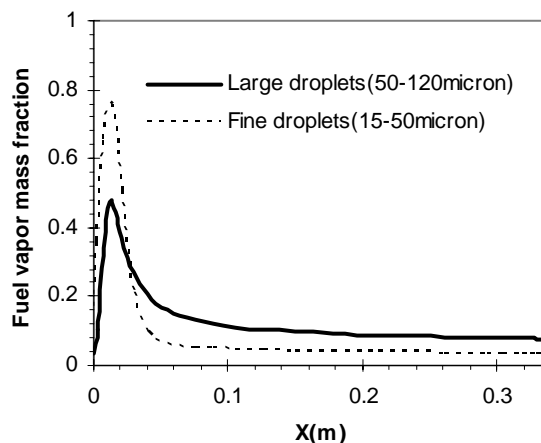


Fig. 6. Centerline distribution of fuel vapor mass fraction along the combustor for the two droplet group sizes

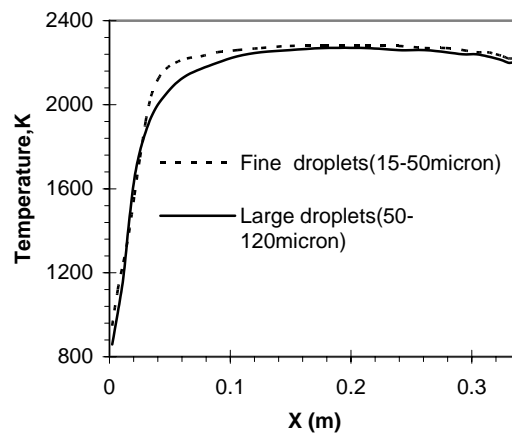


Fig. 7. Centerline distribution of temperature along the combustor for the two droplet group sizes

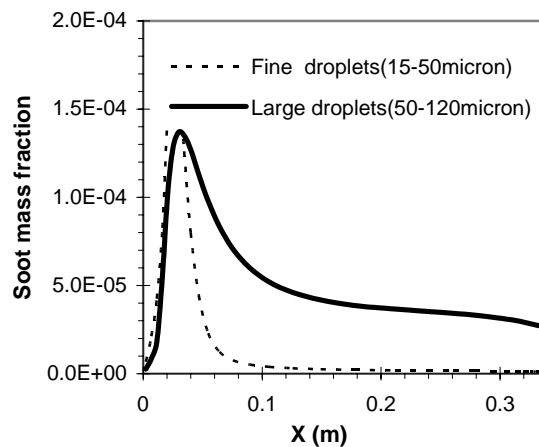


Fig. 8. Centerline distribution of soot mass fraction for the two droplet group sizes

Variations of soot emission for the two droplet group sizes under different equivalence ratios are shown in Fig. 9. The figure reveals that under all equivalence ratios, soot emission remains higher for the large droplets. The figure also shows a significant influence of equivalence ratio on soot emission. As it is clear from the figure, for fuel-lean conditions soot emission from the combustor is negligible, while it rises with increase in the equivalence ratio. Due to Tesner's model (Eqs. (14, 15)) soot formation exponentially increases with temperature. Thus, the considerable reduction of temperature occurring in highly-rich mixtures decreases the formation and emission as can be observed from Fig. 9. This fact has also been reported in previous studies of Moghiman and his co-workers [5].

Figure 10 shows the variations of soot emission for the two droplet group sizes under different inlet air preheat temperatures. As can be observed from the figure, although increase in the inlet air temperature raises soot formation, the rates of increase are nearly the same for the two droplet group sizes and under all temperatures, emission of soot remains higher for the large droplets. It is worth noting that increase in soot formation with temperature occurs as a result of enhanced rates of chemical reactions leading to soot, as concluded by Santoro and Richardson [25].

Figure 11 depicts the variations of soot emission for the two droplet group sizes under different wall temperatures. The figure clarifies that under all wall temperatures, emission of soot is higher for the large droplets. Also, increase in the temperature raises soot emission from the combustor. This matter is a result

of the increased level of temperature inside the combustor due to radiative heat exchange and is in agreement with the previous work of Moghiman and his co-workers in the combustion of natural gas [6].

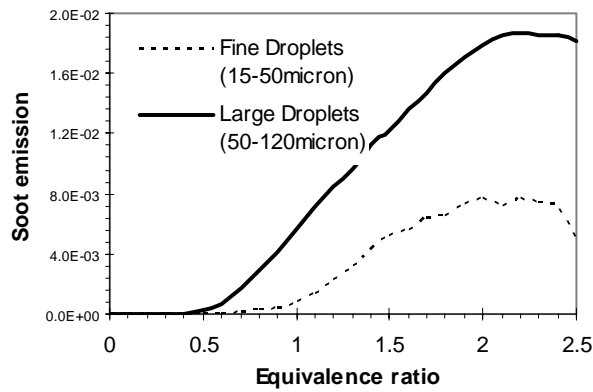


Fig. 9. Variations of soot emission for the two droplet group sizes under different equivalence ratios

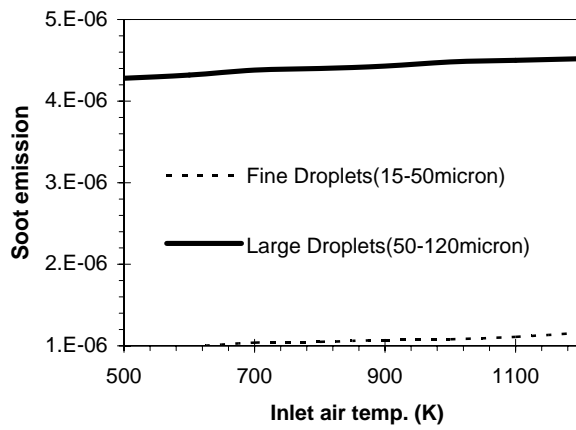


Fig. 10. Variations of soot emission for the two droplet group sizes under different inlet air temperatures

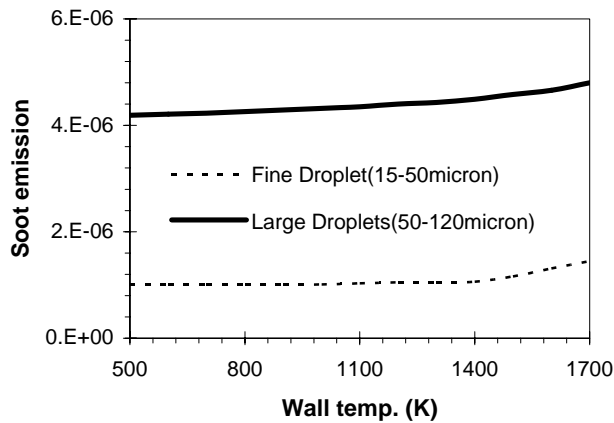


Fig. 11. Variations of soot emission for the two droplet group sizes under different wall temperatures

5. CONCLUSIONS

A numerical simulation of a soot process in a liquid-fuelled combustor was carried out to study the influence of droplet size on the formation and emission of soot. This effect was investigated under different equivalence ratios, inlet air temperatures, and combustor wall temperatures. Soot formation was modeled by a two-step model, which predicts the generation of radical nuclei and then computes the formation of soot from these nuclei. Also, the combustion of soot was modeled by a finite rate combustion model with the eddy dissipation concept. Based on the presented results, the following conclusions may be drawn:

- Droplet size has a significant influence on the soot emission from turbulent spray flames.
- Larger droplets produce higher soot emission than the finer ones.
- Decrease in the size of fuel droplets increases the concentration of soot in the vicinity point of the issue but, due to faster evaporation and combustion of finer droplets, soot concentration decreases rapidly.
- For fuel-lean conditions, soot emission from the combustor is negligible, while it rises with increase in the equivalence ratio.

An increase in the inlet air temperature and wall temperature raises the temperature level inside the combustor which leads to a higher soot emission.

NOMENCLATURE

| | |
|-------------|---|
| A_0 | pre-exponential rate constant |
| a | absorption coefficient |
| a_m | modified absorption coefficient |
| b | size parameter of Rosin-Rammler |
| B | transfer number |
| b_1 | empirical coefficient |
| b_T | empirical coefficient |
| c_p | specific heat |
| $m_{F,s}$ | fuel vapor mass fraction at the particle surface |
| d | droplet diameter |
| D_{eff} | effective mass diffusivity |
| E_b | black body radiation |
| $F-G$ | linear branching-termination coefficient |
| h | enthalpy in Eq. (5) and heat transfer coefficient in Eq. (23) |
| m | mass fraction |
| M | molecular weight |
| Pr | Prandtl number |
| r | radial direction |
| R_r | radiant flux in r -direction |
| R_x | radiant flux in x -direction |
| Re_d | droplet Reynolds number |
| s | stoichiometric coeffi. [Eqs. (10,19)] & scattering coeffi. [Eqs. (7,8)] |
| Sw | swirl number |
| \dot{S} | gas phase mass source term due to evaporation of fuel droplets |
| \dot{S}_j | species conservation equation source term of the j th specie |
| \dot{S}_h | gas phase energy conservation equation source term |
| T | mean temperature |

| | |
|-----|---------------------------|
| u | axial velocity component |
| v | radial velocity component |
| w | swirl velocity |
| x | axial direction |

Greek letters

| | |
|----------------|--|
| α | empirical coefficient |
| β | empirical coefficient |
| α_{eff} | effective thermal diffusivity |
| μ | molecular viscosity |
| ρ | gas phase density |
| η_0 | rate of spontaneous generation of nuclei |
| λ_0 | linear termination on soot particles |

Superscript

| | |
|-----|-----------|
| d | droplet |
| g | gas phase |

Subscript

| | |
|------|------------|
| F | fuel vapor |
| Ox | oxygen |
| N | nuclei |
| S | soot |

REFERENCES

1. Wang, L., Haworth, D. C., Turns, S. R. & Modest, M. F. (2005). Interactions among soot, thermal radiation, and NO_x emissions in oxygen-enriched turbulent nonpremixed flames: a computational fluid dynamics modeling study. *Combustion and Flame*, 141, 170–179.
2. Yang, B., & Koylu, U. O. (2005). Detailed soot field in a turbulent non-premixed ethylene/air flame from laser scattering and extinction experiments. *Combustion and Flame*, 141, 55–65.
3. Lee, E. J., Oh, K. C. & Shin, H. D. (2005). Soot formation in inverse diffusion flames of diluted ethane. *Fuel*, 84, 543–550.
4. Smooke, M. D., Mcenally, C. S., Pefferle, L. D., Hall, R. J. & Colket, M. B. (1999). Computational and experimental study of soot formation in a coflow laminar diffusion flame. *Combustion and Flame*, 117, 117-139.
5. Moghiman, M., Greunberger, T. M., Bowen, P. J. & Syred, N. (2002). Dynamics of soot formation by turbulent combustion and thermal decomposition of natural gas. *Combustion Science and Technology*, 174, 67-86.
6. Moghiman, M. & Greunberger, T. M. (2002). Experimental and computational studies of soot formation in a gas fuelled stabilized combustor. *Iranian Journal of Science and Technology, Transaction B*, 26(B3), 54.
7. Sommerfeld, M. & Qiu, H. H. (1998). Experimental studies of spray evaporation in turbulent flows. *Heat and Fluid Flow*, 19, 10-22.
8. Sornek, R. J., Dobashi, R. & Hirano, T. (2000). Effect of turbulence, mixing, and combustion of liquid-fuel sprays. *Combustion and Flame*, 120, 479–491.
9. Xu, G., Ikegami, M., Honma, S., Ikeda, K., Ma, X., Nagaishi, H., Dietrich, D. L. & Struk, P. M. (2003). Inverse influence of initial diameter on droplet burning rate in cold and hot ambiances: a thermal action of flame in balance with heat loss. *Heat and Mass Transfer*, 46, 1155-1169.

10. Lefebvre, A. H. (1975). Pollution control in continuous combustion engines. *15th Symposium (International) on Combustion*, 1169-1180.
11. German, A. E. & Mahmud, T. (2005). Modelling of non-premixed swirl burner flows using a Reynolds-stress turbulence closure. *Fuel*, 84, 583-594.
12. Zhang, J., Nieh, S. & Zhou, L. (1992). A new version of algebraic stress model for simulating strongly swirling flows. *Numerical Heat Transfer, Part B, Vol. 22*, 49-55.
13. Gosman, A. D. & Lockwood, F. C. (1973). Incorporation of a flux model for radiation into a finite difference procedure for furnace calculations. *14th Symposium (International) on Combustion*, 661.
14. Magnussen, B. F. & Hjertager, B. H. (1976). Mathematical models of turbulent combustion with special emphasis on soot formation and combustion. *16th symposium (International) on Combustion*, 719.
15. Tesner, P. A., Snegiriova, T. D. & Knorre, V. G. (1971). *Kinetics of dispersed carbon formation*. Combustion and Flame, 253.
16. Okuyama, M., Echigo, R. Hanamura, K., Yoshida, H., Koda, M. & Koganezawa, T. (2004). *Modeling of soot particles growth in fuel-rich premixed flame*, *Heat and Mass Transfer*, 47, 4625-4635.
17. Cheung, S. C. P., Yuen, R. K. K., Yeoh, G. H. & Cheng, G. W. Y. (2004). Contribution of soot particles on global radiative heat transfer in a two-compartment fire. *Fire Safety*, 39, 412-428.
18. Sharma, N. Y. & Dom, S. K. (2004). Influence of fuel volatility and spray parameters on combustion characteristics and NOx emission in a gas turbine combustor. *Applied Thermal Engineering*, 24, 885-903.
19. Hinds, W. C. (1999). *Aerosol Science and Technology*. Wiley, New York, 1999.
20. Saario, A., Rebola, A., Coelho, P. J., Costa, M. & Oksanen, A. (2005). Heavy fuel oil combustion in a cylindrical laboratory furnace: measurements and modeling. *Fuel*, 84, 359-369.
21. Faeth, G. M. (1983). Evaporation and combustion of sprays. *Progress in Energy and Combustion Sciences*, 9.
22. Versteeg, H. K. & Malalaseke, W. (1996). *An introduction to computational fluid dynamics- The finite volume method*. Longman Scientific & Technical.
23. Moghiman, M. & Maneshkarimi, M. R. (2001). On the dependence of spray evaporation and combustion on atomization techniques. *Iranian Journal of Science and Technology, Transaction B*, 25, (B2).
24. Khalil, E. E. (1982). *Modeling of furnaces and combustors*. Cairo University Press.
25. Santoro, R. J. & Richardson, T. F. (1994). *Concentration and temperature effects on soot formation in diffusion flames, Detailed mechanism and modeling of soot formation*. In: Bockhorn, H.(ed.), Soot formation in combustion: mechanisms and models, Springer, 221-239.